ACS Chemical Neuroscience

pubs.acs.org/chemneuro Research Article

Optical Control of Adenosine A_{2A} Receptor Using Istradefylline Photosensitivity

Anaëlle Dumazer, Xavier Gómez-Santacana, Fanny Malhaire, Chris Jopling, Damien Maurel, Guillaume Lebon, Amadeu Llebaria,* and Cyril Goudet*

Cite This: https://doi.org/10.1021/acschemneuro.3c00721 Read Online

ACCESS | Metrics & More | Article Recommendations | Supporting Information

ABSTRACT: In recent years, there has been growing interest in the potential therapeutic use of inhibitors of adenosine A_{2A} receptors ($A_{2A}R$) for the treatment of neurodegenerative diseases and cancer. Nevertheless, the widespread expression of $A_{2A}R$ throughout the body emphasizes the importance of temporally and spatially selective ligands. Photopharmacology is an emerging strategy that utilizes photosensitive ligands to attain high spatiotemporal precision and regulate the function of biomolecules using light. In this study, we combined photochemistry and cellular and in vivo photopharmacology to investigate the light sensitivity of the FDA-approved antagonist istradefylline and its potential use as an $A_{2A}R$ photopharmacological tool. Our findings reveal that istradefylline exhibits rapid trans-to-cis isomerization under near-UV light, and prolonged exposure results in the formation of photocycloaddition products. We demonstrate that exposure to UV light triggers a time-dependent decrease in the antagonistic activity of istradefylline in $A_{2A}R$-expressing cells and enables real-time optical control of $A_{2A}R$ signaling in living cells and zebrafish. Together, these data demonstrate that istradefylline is a photoinactivatable $A_{2A}R$ antagonist and that this property can be utilized to perform photopharmacological experiments in living cells and animals.

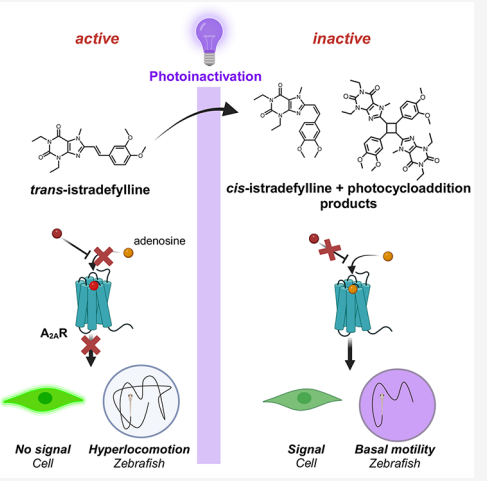

KEYWORDS: *photopharmacology, GPCR, photoswitch, purinergic, adenosine*

INTRODUCTION

G protein-coupled receptors (GPCRs) are a superfamily of more than 800 membrane proteins, which are key players in cell communication.[1,2] With more than a third of the drugs on the market directed against them, GPCRs are attractive therapeutic targets.[3,4]

Among GPCRs, the adenosine receptor family has attracted a lot of interest for their therapeutic potential in neurodegenerative, inflammatory, and autoimmune diseases, cardiac ischemic diseases as well as chronic pain, sleep disorders, and cancer.[5,6] The family is composed of four members (A_1R, $A_{2A}R$, $A_{2B}R$, and A_3R), with different pharmacological, signaling, and expression profiles.[5] More particularly, the A_{2A} subtype is a recognized target for the treatment of Parkinson disease (PD)[7,8] and cardiovascular diseases[9] and is a promising target for cancer immunotherapy,[10,11] pain,[12] and Alzheimer's disease.[13] So far, three drugs targeting this receptor have received FDA approval. The endogenous ligand adenosine[14] and the synthetic selective $A_{2A}R$ agonist regadenoson[15] are used in clinics as vasodilator agents, while the $A_{2A}R$ antagonist istradefylline (also named KW-6002) has been approved as an adjunctive treatment for PD in combination with levodopa in Japan and USA.[16,17] Istradefylline is a styryl-xanthine analogue related to caffeine. It is a selective and potent competitive $A_{2A}R$ antagonist.[18] In addition, several studies reported that istradefylline could also be therapeutically used as a potential drug for Alzheimer disease,[13] since it reduces memory deficits in aging mice with amyloid pathology[19] and enhances amyloid-β generation and γ-secretase activity.[20]

A common difficulty in pharmacology comes from the broad expression of a given target, which emphasizes the need for temporally and spatially selective drugs to reduce the risk of side effects. This is well illustrated by $A_{2A}R$ that is not only present in the central nervous system, where it is highly expressed in the striatum and at lower expression levels in the cerebral cortex and in the hippocampus, but also in the immune system, heart, and lungs.[5] One way to circumvent this difficulty is photopharmacology, an emerging light-based strategy to manipulate biological processes with high spatiotemporal precision.[21,22] This relies on the use of photosensitive ligands, which allows the photocontrol of the

Received: November 6, 2023
Revised: December 21, 2023
Accepted: January 3, 2024

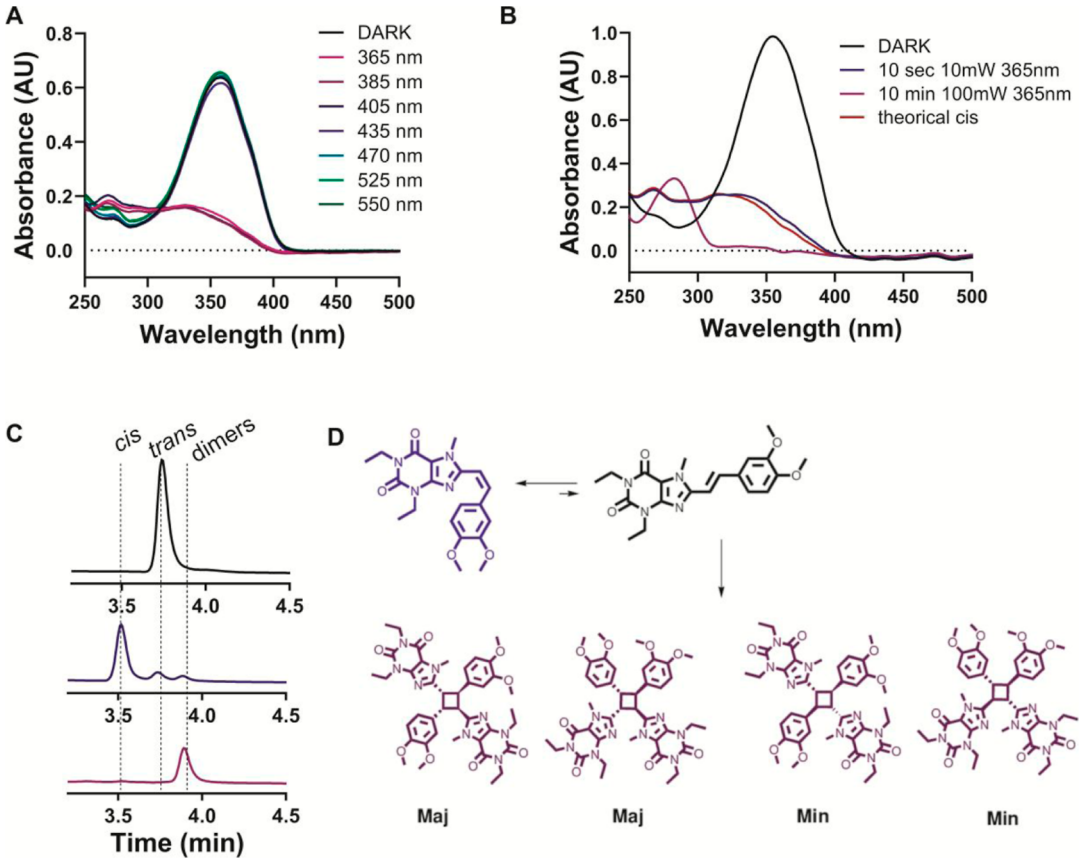

Figure 1. Photochemical characterization of istradefylline light sensitivity. (A) Absorption spectrum of istradefylline (100 μM in PBS, 1% DMSO) after 10 s illumination with different wavelengths at 10 mW. (B) Absorption spectrum of istradefylline, 25 μM in PBS (20% DMSO) in the dark and after different time and power of 365 nm UV-light illumination. (C) HPLC of the corresponding samples of panel (B); top: dark, middle: 10 s, 10 mW, 365 nm, bottom: 10 min, 100 mW, 365 nm. (D) Chemical structures of the photoreaction products of istradefylline after illumination with near-UV light: trans-istradefylline in black (corresponding to the peak at t = 3.73 min in the HPLC chromatograms), cis-istradefylline in blue (HPLC t = 3.52 min), and the group of dimers (HPLC t = 3.89 min).

drug−target interaction and its consequent biological activity. Two major categories of photosensitive ligands are available, photoactivatable ligands (also named caged ligands),[23] which are irreversibly activated by light, and photochromic or photoswitchable ligands,[24] which can be reversibly switched from an active to an inactive conformation. Combined with optical technologies, photopharmacology is a powerful fundamental research tool to explore the physiopathological function of endogenous regulatory systems, with micrometric spatial resolution and millisecond temporal resolution, opening new pharmacotherapeutic opportunities toward precision medicine.[25,26] Increasing interest is being shown in GPCR photopharmacology,[27,28] which offers the possibility to modulate and understand GPCR physiology and pathology with a higher spatiotemporal control than that offered by classical pharmacological approaches. Photopharmacology has been applied to many GPCRs including dopamine,[29] cannabinoid,[30,31] opioid,[32,33] glutamate,[34] and adrenergic receptors.[35,36] Concerning adenosine receptors, a photoactivatable $A_{2A}R$ antagonist, MRS7145,[37] a nonselective photoswitchable partial agonist, MRS5543,[38] and an adenosine-based photoswitchable agonist, AA-3[39] have been reported. Exploration of the pathophysiological function of $A_{2A}R$ and its therapeutic potential may benefit from additional selective $A_{2A}R$ photochromic ligands.

In this study, seeking novel photopharmacological tools for $A_{2A}R$, we combined photochemistry and cellular and in vivo photopharmacology to carry out an in-depth investigation of the light sensitivity of the well-known $A_{2A}R$ antagonist istradefylline and its potential use in photopharmacology. Previous studies have shown that prolonged exposure of istradefylline to daylight induces an isomerization of its heterostilbene olefinic bond from trans to cis, resulting in a strong reduction of its affinity for the receptor.[40] Here, we confirm the sensitivity of istradefylline to illumination and, in particular, to near-UV light, which rapidly turns it from its active trans isomer to the inactive cis isomer and irreversibly leads toward four fully $A_{2A}R$ inactive photoproducts. We then demonstrate that illumination by UV light can rapidly suppress the istradefylline-induced blockade of $A_{2A}R$ cellular signaling and abolish the istradefylline-mediated hyperlocomotor activity induced by the $A_{2A}R$ blockade in zebrafish larvae. Taken together, our experiments indicate that istradefylline is a photoinactivatable $A_{2A}R$ antagonist and that this property can be used for the optical control of $A_{2A}R$ in cells and living organisms.

RESULTS

Istradefylline Exhibits Rapid Trans-to-Cis Isomerization under Near-UV Light, While Prolonged Exposure Leads to the Generation of Photocycloaddition

https://doi.org/10.1021/acschemneuro.3c00721
ACS Chem. Neurosci. XXXX, XXX, XXX−XXX

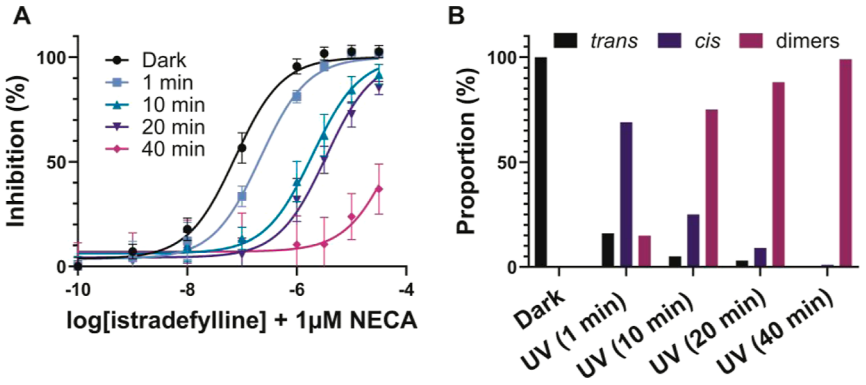

Figure 2. Influence of UV light on istradefylline photoisomerization and photoreaction and its capacity to inhibit $A_{2A}R$ function in cells. (A) The influence of UV light on the ability of istradefylline to inhibit agonist-induced activity of adenosine A_{2A} receptor was determined by measuring the production of cAMP in CHO cells stably expressing the human $A_{2A}R$. Experiments were performed in the presence of a fixed dose of the agonist NECA (1 μM) and different doses of istradefylline, in the dark or after 365 nm illumination at 10 mW for different exposure times (1−40 min, as indicated). Data are mean ± SEM of n = 5 and n = 3 independent experiments in dark and UV light conditions, respectively. (B) Estimation of the proportion of trans, cis, and dimers after illumination in the same conditions than in A, determined by HPLC from chromatograms displayed at the wavelength of the two isosbestic points trans−cis and trans-dimers.

Products. Istradefylline, along with other styryl-xanthines, is known to photoisomerize from trans to the corresponding cis isomer and vice versa following prolonged illumination with visible light, with a photostationary state obtained between 1.5 and 24 h depending on the solvent and the concentration used.[41,42]

First, we determined whether the illumination time to reach a photostationary state could be reduced by the use of wavelength-specific light. To this end, we illuminated 100 μM istradefylline samples for 10 s with different wavelengths, ranging from 365 to 550 nm at 10 mW, and measured the UV−visible absorption spectrum in phosphate-buffered saline (PBS) [20% dimethyl sulfoxide (DMSO)]. This revealed that near-UV light drastically affects the absorption spectrum in the direction of the disappearance of the trans isomer (Figure 1A). In order to better define the kinetics and nature of the photoreaction, we then monitored the absorption spectrum of istradefylline after exposure to UV light at different times and power levels. Interestingly, we observed a substantial change in the spectrum coherent with a mixture of trans and cis isomers, with an isosbestic point found at 304 nm (Figure S1), after only 5 s of illumination with a 365 nm light-emitting diode (LED) light at 10 mW. Illuminating for 5 more seconds slightly changed the absorption spectrum, mainly by reducing the absorbance between 350 and 370 nm due to the decrease of the trans isomer (Figure 1B). Based on high-performance liquid chromatography−mass spectrometry (HPLC−MS) analysis (Figure S2), it was confirmed that these conditions of illumination mainly led to cis-istradefylline (∼93%), with only few remaining trans isomers (∼5%) (Figure 1C). Of note, a new peak of low intensity at higher retention time was obtained. When illuminating for a longer period and with a higher power (100 mW), the UV−vis absorption spectrum changed again with a blue-shift of the absorption maximum of 283 nm (Figure 1B). The HPLC−MS showed the total disappearance of the peaks corresponding to the cis and the trans isomers but not the peak at higher retention time that corresponds to a mixture of products (Figure 1C), all of them having a molecular mass (m/z) of 769.5. This mass is consistent with the dimerization of istradefylline as a result of a [2 + 2] photocycloaddition of the trans-isomer to form several cyclobutane adducts (Figure 1D), as previously reported in solid state.[40] The formation of stilbene photocycloaddition products from the cis-isomers is generally discarded because the cis-stilbene has an S_1 state that is much too short-lived to complete the cycloaddition reaction.[43] HPLC−MS analysis of the separated cyclobutane analogues obtained under our conditions indicated the existence of at least three different cyclobutane isomers. To identify the structure of the cyclobutane dimers obtained in solution, we illuminated a concentrated solution of istradefylline in DMSO. Preparative HPLC allowed us to separate the three main HPLC peaks corresponding to the dimers. The first fraction (**dimer 1**) appears to be a mixture of two dimers that account for 7% of the total mass of dimers obtained after the purification. The second (**dimer 2**) and third fractions (**dimer 3**) correspond to two pure photocycloaddition products, accounting, respectively, for 45 and 48% of the total mass of dimers after the purification. The structures of the compounds obtained from the two major fractions were determined by proton nuclear magnetic resonance (^{1}H NMR) and carbon nuclear magnetic resonance(^{13}C NMR) (Figure S3). **Dimer 2** corresponds to the syn-head-to-tail cyclobutane isomers, previously identified in solid state by the group of Müller,[40] whereas the others have a distinct structure. According to the literature, both head-to-head and head-to-tail isomers are favored; therefore, we assumed that **dimer 3** is the syn-head-to-head cyclobutane derivative. Besides, NMR spectra of similar [2 + 2] photocycloaddition products[44,45] confirm our hypothesis (Figure S4). The small quantity obtained for **dimer 1** allowed us to record only an ^{1}H NMR spectrum. Based on the comparison between the ^{1}H NMR signals obtained for the cyclobutane protons and cyclobutanes obtained in the literature, we tentatively identify them as originating from the less-favored [2 + 2] photocyclization anti head-to-head and head-to-tail dimeric pairing of two istradefylline molecules.

UV-Light Exposure Time-Dependently Decreases the Antagonistic Activity of Istradefylline on $A_{2A}R$. We next assessed the activity of istradefylline at $A_{2A}R$ at different stages of the phototransformation. The geometric isomers (i.e., cis/trans) and the different irreversible cycloalkane photoproducts were obtained from istradefylline samples exposed to different UV-illumination times. The conditions of illumination were set up in order to be compatible with an analysis of the samples by

https://doi.org/10.1021/acschemneuro.3c00721
ACS Chem. Neurosci. XXXX, XXX, XXX−XXX

HPLC−MS. Stock samples in DMSO (2 μL at 10 mM in DMSO) were illuminated with a 365 nm LED source set at 10 mW for 1, 10, 20, and 40 min. Then, these samples were tested in CHO cells stably expressing the human $A_{2A}R$. Since $A_{2A}R$ couple $G_{\alpha s}$ family members, which activate adenylyl cyclase, the cytosolic cAMP concentration was recorded using an end point time-resolved fluorescence energy transfer (TR-FRET)-based cyclic adenosine monophosphate (cAMP) accumulation assay to account for $A_{2A}R$ activation. To assess the antagonistic activity of istradefylline at different times of illumination, $A_{2A}R$-expressing cells were coincubated with a fixed concentration of the agonist 5'-N-ethylcarboxamidoadenosine (NECA) (1 μM) and increasing concentrations of the different istradefylline samples. A large difference in the IC_{50} values was observed between the istradefylline sample kept in the dark and the illuminated samples as we observed a large rightward shift of the inhibition curve (Figure 2A). The 1 min preilluminated sample displays a modest difference of potency (3-fold), whereas the 20 min illuminated sample shows a strong difference of potency (41-fold), as compared to that of the istradefylline sample in the dark (Figure 2C and Table 1).

Table 1. Potencies and Proportion of Isomers and Photoproducts in the Dark and Following Different Exposure Times at 365 nm[a]

	IC_{50} (μM)	$IC_{50\ illum}/IC_{50\ dark}$	% trans	% cis	% dimers
dark	0.07 ± 0.02		100	0	0
1 min	0.24 ± 0.01	3	16	69	15
10 min	1.9 ± 0.6	27	5	25	70
20 min	2.7 ± 1.1	39	3	9	88
40 min	25.7 ± 5.1	367	<0.5	1	99

[a]IC_{50} and ratio of IC_{50} of istradefylline were determined using a cAMP accumulation assay in CHO cells stably expressing the human $A_{2A}R$. Experiments were performed in the presence of a fixed dose of the agonist NECA (1 μM) and different doses of istradefylline that have been protected from light (dark) or illuminated with a 365 nm LED (10 mW) for different exposure times (1−40 min, as indicated). Data are mean ± SEM of at least 3 independent experiments. Percentage of trans, cis, and dimer entities were calculated from the HPLC analysis of the illuminated samples (365 nm; 10 mW), from chromatograms displayed at the wavelength of the two isosbestic points trans−cis and trans-dimers.

To estimate the proportion of the mixture of dimers and trans and cis isomers in each sample, an analysis was performed from the HPLC−MS istradefylline samples illuminated in the same illumination conditions as for the cell assay (Figure S5 and Table S1). As previously shown in a diluted aqueous solution, we first observed by HPLC−MS analysis a fast decrease of the trans isomer fraction and a concomitant increase in the cis isomer. Extending the photoreaction time results in the accumulation of irreversible [2 + 2]-cycloaddition photoproducts (Figure 2B). After 10 min of illumination, only 5% of the initial trans istradefylline remains in the solution (Table 1). We estimate the theorical IC_{50} of the 5% of remaining $A_{2A}R$ active istradefylline trans isomer to an apparent IC_{50} of 1.4 μM, close to the potency determined experimentally (IC_{50} = 11.9 ± 0.6 μM). It is also the case for the 20 min illumination sample, where 3% of the remaining trans-istradefylline leads to a theoretical IC_{50} of 2.3 μM, located in the range of the experimental data (IC_{50} = 2.7 ± 1.1 μM). These results suggest that almost all the remaining antagonistic activity of the preilluminated samples is due to the residual trans isomer, meaning that the cis isomer has a lower antagonistic potency for $A_{2A}R$. It is consistent with the results obtained by the group of Suzuki[41] in which they reported a 800-fold higher activity of the trans isomer compared to that of the cis isomer, in a styryl-xanthine molecule similar to istradefylline. Of note, we attempted to obtain a purified cis isomer, which turns out to have a low bistability and relaxes thermally to the trans isomer. Therefore, the isolated sample contained a small amount (14%) of the trans isomer, precluding its use in a pharmacological assay to precisely determine the cis isomer activity (Figure S6).

All these experiments show that istradefylline is antagonizing $A_{2A}R$ only in its trans configuration and that light can be used to convert it to the inactive cis isomer or dimeric photoproducts.

Istradefylline Enables Real-Time Optical Control of $A_{2A}R$ Cellular Signaling. Next, we wanted to take advantage of this rapid light-induced loss of istradefylline activity to dynamically regulate $A_{2A}R$ activity in cells. To assess real-time $A_{2A}R$ cell signaling, a double stable cell line containing both the $A_{2A}R$ and the cAMP fluorescent indicator Flamindo2 was developed. Flamindo2 is a yellow fluorescent protein-based cAMP indicator[46] that has an absorption peak at 480 nm and emission maximum at 510 nm, which are fully compatible with istradefylline photochemistry. Flamindo2 fluorescence is inversely correlated with the cAMP concentration, decreasing as the cAMP concentration increases (Figure 3A). As shown in Figure 3B, a dynamic and dose-dependent decrease of fluorescence can be measured following the activation of $A_{2A}R$ by the agonist NECA. The potency of NECA extrapolated from experimental analysis (pEC_{50} = 21 ± 6 nM) is consistent with the results obtained with other cell-based assays (Figure 3C).

We then tested whether **dimers 1**, **dimer 2**, and **dimer 3** have an antagonistic activity at $A_{2A}R$. The three dimeric products isolated from a photoreaction (10 μM), trans-istradefylline (10 μM, kept in the dark), the antagonist XAC (10 μM), or buffer were applied 3 min prior to the addition of 1 μM of NECA to initiate the production of cAMP. The signals were analyzed by integrating the area under each curve and were normalized to the NECA-induced response alone (0% inhibition) and the signal with the vehicle alone (100% inhibition) (Figure 3D). We did not observe an inhibition of the NECA-induced response by any of the photoreaction dimers at 10 μM, while trans-istradefylline and XAC at the same concentration reached 86 and 98% inhibition, respectively.

Next, we assessed the light-dependent activity of istradefylline. Cells were preincubated with the photochemically stable antagonist XAC, with istradefylline or vehicle (baseline) for 4.5 min. During this period, the cells were kept in the dark or illuminated for 30 s at 395 nm. Then, the agonist NECA was added to induce cAMP production following $A_{2A}R$ activation. The fluorescence intensity (FI) was recorded during all the experiments, except during the 30 s of illumination (Figure 3E). The signal was normalized and corrected to the baseline to compensate for the loss of fluorescence over time caused by photobleaching. In dark conditions, we can clearly observe a reversion of NECA induced-signal in similar proportions for istradefylline and XAC (Figure 3F), while the antagonistic activity of istradefylline is abolished following UV illumination. On the other hand, the antagonistic effect of XAC remains unaltered in both dark or illuminated conditions. This

https://doi.org/10.1021/acschemneuro.3c00721
ACS Chem. Neurosci. XXXX, XXX, XXX−XXX

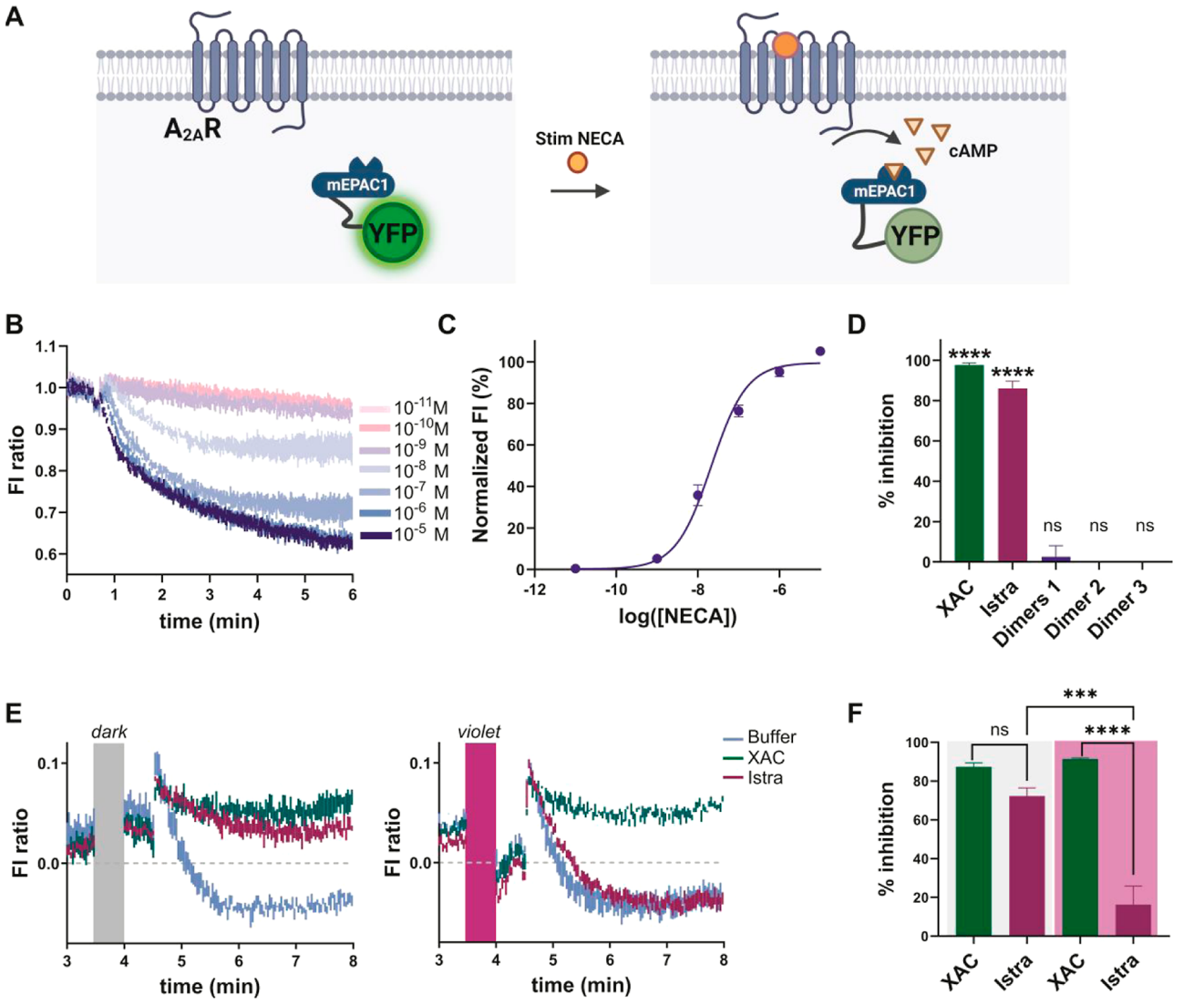

Figure 3. Influence of UV light on istradefylline inhibition on real-time $A_{2A}R$ cellular signaling. (A) Principle of the fluorescence-based assay in the CHO-$A_{2A}R$-Flamindo2 cell line. FI of Flamindo2 decreases as the intracellular cAMP concentration increases. (B) Time-course of FI following $A_{2A}R$ stimulation with different concentrations of the agonist NECA in the CHO-$A_{2A}R$-Flamindo2 cell line. (C) Dose−response curve of NECA, as determined from panel (B). The peak of FI in the absence of NECA was normalized to 0%, and the peak in the presence of 10 μM NECA was normalized to 100%. All data points represent the mean ± SEM of four independent experiments. (D) Quantification of the percentage of receptor inhibition with 10 μM of XAC, istradefylline, and the three purified dimers. Data are mean ± SEM of at least four independent experiments. (E) Time-course of FI induced by 1 μM NECA in CHO-$A_{2A}R$-Flamindo2 cells, alone (blue trace) or in the presence of 1 μM of istradefylline (violet trace) or 1 μM of the nonphotosensitive A_{2A} antagonist XAC (green trace), with 30 s dark or violet light (395 nm, 14 mW) treatment (left and right panels, respectively). This experiment is representative of three individual experiments. (F) Quantification of the percentage of receptor inhibition with antagonists following dark or UV treatment. Data are presented as mean ± SEM of $n = 5$ and $n = 3$ experiments for istradefylline and XAC, respectively. Data were analyzed by a one-way analysis of variance (ANOVA) followed by Dunnett's post hoc test. ***$p < 0.005$, ****$p < 0.001$.

demonstrates that it is possible to dynamically abolish the antagonistic effect of istradefylline on $A_{2A}R$ cell signaling by controlling the UV-light-induced phototransformation of istradefylline.

UV Light Abolishes Istradefylline-Induced Hyperlocomotion in Zebrafish Larvae. We next assessed whether we can use istradefylline photosensitivity to control $A_{2A}R$ in vivo with light using zebrafish larvae. Their transparency makes them ideal models for manipulating photosensitive compounds in vivo.[47] Zebrafish possess two $A_{2A}R$ genes named adora2a.1 and adora2a.2, which share 62 and 74% amino acid identity to mammalian $A_{2A}R$, respectively.[48] The key residues involved in the binding of istradefylline on human $A_{2A}R$[49] are conserved in zebrafish orthologs. Since blockade of $A_{2A}R$ receptors has been previously reported to increase zebrafish locomotion,[50] we evaluated the influence of light on the effect of istradefylline on the free-swimming behavior of naïve 5 day old zebrafish larvae.

We used a conventional locomotion assay on zebrafish larvae coupled to an LED illumination system to measure locomotion after direct addition of the compounds in the medium, either in the dark or under illumination with violet light (385 nm) (Figure 4A). Istradefylline in its trans configuration increased larvae motility 2-fold, while the istradefylline sample that has been preilluminated (365 nm, 10 mW, 2 min) had no effect on motility (Figure 4C, left) in agreement with the $A_{2A}R$ activity that we recorded in cell-based assays. Under these illumination

https://doi.org/10.1021/acschemneuro.3c00721
ACS Chem. Neurosci. XXXX, XXX, XXX−XXX

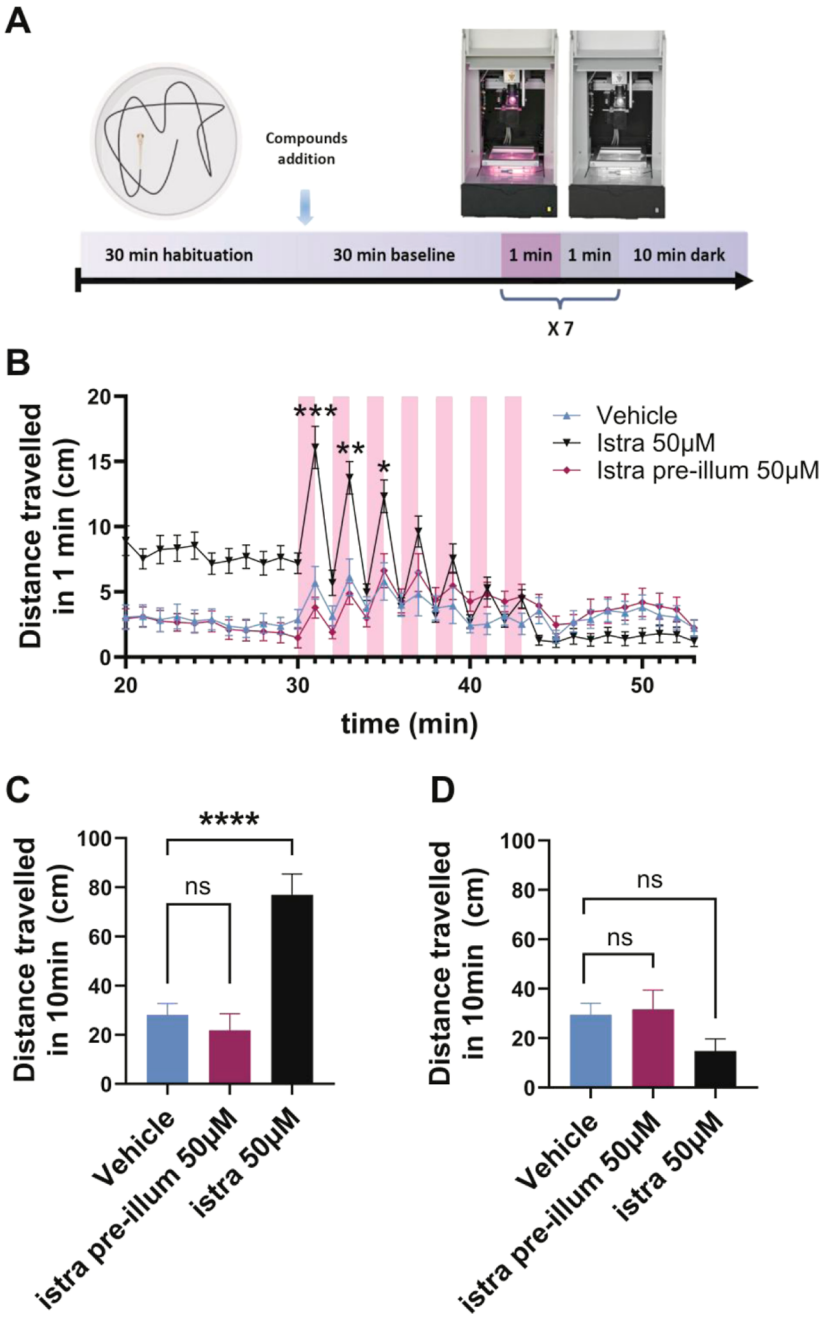

Figure 4. Influence of UV light on istradefylline-induced hyperlocomotion in zebrafish. (A) Experimental timeline: one 5 day old zebrafish larva was placed in a well of a 96-well plate. Following 30 min of habituation, larvae were exposed for 30 min to vehicle (DMSO 0.5%), 50 μM istradefylline (kept in the dark), or 50 μM UV-pretreated istradefylline (Istra preillum), directly added to the well. After 30 min, zebrafish received seven UV/dark illumination cycles (1 min UV (365 nm, 8 mW) and 1 min dark). (B) Integration of the total free-swimming distance for every minute. Each data point corresponds to the mean ± SEM of the total distance swum during 1 min by 15−16 zebrafish larvae. (C,D) Cumulative distance traveled in 10 min by the zebrafish larva treated with vehicle, istradefylline, or preilluminated istradefylline, before (C) and after (D) the illumination cycles. Each data point corresponds to the mean ± SEM of the total distance swum during 10 min by 15−16 zebrafish larvae. Data shown correspond to a representative experiment from 3 independent experiments. Statistics were performed with a one-way panel (C) or a two-way panel (B) ANOVA followed by Dunnett's multiple comparison test. *$p < 0.05$, **$p < 0.01$, ***$p < 0.005$.

conditions, HPLC−MS analysis indicated that the solution contains a majority of dimers (~75%), some cis isomers (~24%), and 1% of trans isomer (Figure S7, Tables S2 and S3). UV light by itself enhanced the swimming behavior of the larvae (Figure 4B), as shown in experiments with zebrafish and light in previous reports.[47,51] This effect is exacerbated in the presence of the active trans isomer, where UV-induced hyperlocomotion and istradefylline-induced hyperlocomotion are additive while maintaining a ratio of around 2.2 between the distance traveled under illumination vs the distance without illumination (Figure 4B). However, the istradefylline-induced hypermobility is lost after four UV illumination cycles (385 nm, 1 min at 8 mW each cycle) (Figure 4C, right). The conditions of illumination after each of the four first illumination cycles were reproduced and analyzed by HPLC−MS to obtain the ratio of istradefylline isomers and other

https://doi.org/10.1021/acschemneuro.3c00721
ACS Chem. Neurosci. XXXX, XXX, XXX−XXX

photoproducts (Figure S8, Table S2). After the first cycle, only 10% of trans isomer remains, which decreased to 2% after cycle 2 and 3 and further decreased to 1% after cycle 4, the rest being a mixture of cis and dimer photoproducts (Table S3). The loss of istradefylline activity is consistent with conversion from the trans $A_{2A}R$-active form to the less active or inactive cis/photoreaction.

In this series of experiments, we provide evidence that istradefylline activity can be rapidly switched off in vivo in living zebrafish larvae by the application of UV light.

DISCUSSION

In this study, we explored the influence of UV light on istradefylline at the molecular and functional level. We showed that, in solution, near-UV light rapidly triggers the reversible isomerization of the ligand from its active trans isomer to the less active cis isomer and that UV light also mediates its irreversible transformation into fully inactive dimeric photoproducts. Finally, we demonstrated that UV-triggered photoinactivation of istradefylline is compatible with real-time photopharmacological experiments both in vitro and in vivo.

We elaborated the present study based on previous work showing that istradefylline, along with others styryl-xanthines, is photosensitive. Istradefylline was known to isomerize following prolonged illumination with light.[40,42] Moreover, in solid state, Hockemeyer and colleagues reported the occurrence of a [2 + 2] photocycloaddition product after illumination of the sample for 100 min that they identified to be a cyclobutane derivative originating from the syn head to tail dimeric pair of the trans isomers.[40] One of the findings of our study is that after sustained near-UV exposure in solution, we were able to identify four different dimeric cyclobutane photoproducts of istradefylline (Figures 1D and S4). **Dimer 2** corresponds to the previously identified product,[40] whereas **dimers 1** and **dimer 3** have distinct structures that we propose to be a mixture of anti head-to-head and head-to-tail cyclobutane isomers and the pure syn-head-to-head cyclobutane isomer, respectively. In a study from Matsuura group on the [2 + 2] photocyclization of 4-cyanostilbene, the different cyclobutane isomers were obtained in a similar ratio.[52] Altogether, these results demonstrate that light promotes a dynamic equilibrium between trans and cis istradefylline isomers, which under sustained exposure to light mediates the production of four photoproducts, which correspond to the different dimeric cyclobutane analogues of istradefylline.

One of the interesting outcomes from this study is that we can harness the photosensitivity of istradefylline to our advantage and use it as a photoinactivatable antagonist tool in cells or living animals. We demonstrate that the dimeric photoproducts are fully inactive toward $A_{2A}R$ and that exposure to near-UV light rapidly and dramatically decreases the antagonistic activity of istradefylline to $A_{2A}R$, making it compatible for in vivo photopharmacology experiments. This photochemical property can be exploited to obtain localized optical control of $A_{2A}R$ activity with high temporal precision in biological media. In combination with the photoactivable $A_{2A}R$ antagonist MRS7145,[37] the photoinactivatable $A_{2A}R$ antagonist istradefylline provides a complementary light-controlled molecular probe to dynamically study $A_{2A}R$ function. Of interest, istradefylline is a readily available well-characterized clinically proven drug. This powerful and accessible tool could find useful applications to decipher the physiopathological mechanisms related to $A_{2A}R$ activation and inactivation during defined times and at precise locations in cells, ex vivo, and in animal models. For example, it could be possible to block all the A_{2A} receptors in an organism and, with very precise control in space and time, to remove the block at a specific site and observe the associated biological, physiological, or behavioral responses. This study also demonstrates that istradefylline has to be strictly protected from light by users to avoid the photodegradation of the active drug into (trans/cis/photodimer)-istradefylline mixtures. Moreover, photosensitivity has to be considered in the handling, packaging, and storage of this drug. Future studies should be aimed at developing a selective photoswitchable $A_{2A}R$ antagonist that could be reversibly activated and inactivated by light, which would provide an additional temporal dimension to the control of this receptor and expand the range of A_{2A} photocontrollable molecules. Based on our data, we speculate that istradefylline appears to be a good scaffold candidate for its transformation into a selective photoswitchable $A_{2A}R$ antagonist.

The concept of photorepurposing was recently defined by Kobauri et al.[24] as the study of light-induced changes in activity of compounds that were not initially designed for photopharmacology. There are several examples of photorepurposing, such as Plinabulin,[53] a tubulin polymerization inhibitor, and GL479,[54] a dual PPARα/γ agonist, to cite two recent ones, now joined by istradefylline. Considering styril-based compounds, two studies examined the difference in activity between the trans and the cis isomers. The Thorn-Seshold group successfully developed a light-specific styryl-benzothiazole (SBT),[55] a tubulin polymerization inhibitor, by photoconverting the trans inactive isomer into the 200-fold more active cis isomer with fast application of violet light in cells, whole organ and in vivo. More similarly to our study, axitinib, a-styryl heteroarene tyrosine kinase inhibitor marketed for second-line therapy of renal cell carcinoma, displays a phototransformation with UV light.[56] In a vascular endothelial growth factor receptor 2 assay, isolated trans-axitinib was more active than the cis isomer, but the generation of an inactive [2 + 2] photocycloaddition product with UV light prevented reversible switching, leading to a reduction in the activity of the molecule after illumination. Taken together, these data suggest a proof of concept to use certain styryl-based molecules that can undergo a fast isomerization and/or [2 + 2] photocycloaddition with UV light as a way to irreversibly induce a reduction in the activity of the molecule following illumination. It also opens a question on the photostability of stilbene or other functional-group-containing drugs and the possible deleterious effects of light exposure on drug therapeutic treatments.[57−59] Beyond these examples, there are very likely other photoswitch-containing ligands that have the potential to become photopharmacological tools. Notably, considering that the styryl arene or heteroarene group is widely represented in medicinal chemistry,[60] this category could be expanded to include other styryl-arene-based compounds. With its light-induced irreversible loss of activity due to photocycloaddition products, the styril-containing istradefylline has exactly the opposite property to photoactivatable ligands. If more examples of this type were to be discovered, they could therefore constitute a new class of photopharmacological ligands, i.e., photoinactivatable ligands that are irreversibly inactivated by light, allowing rapid, local neutralization of their pharmacological activity, complementing photoactivatable (caged) and photoswitchable ligands.

https://doi.org/10.1021/acschemneuro.3c00721
ACS Chem. Neurosci. XXXX, XXX, XXX−XXX

In conclusion, following an in-depth understanding of the photosensitivity of istradefylline at the molecular level, we propose a new application for istradefylline as a photopharmacological tool. We have established the proof of concept that the blockade of $A_{2A}R$ function by istradefylline can be rapidly abolished by near-UV light in living cells and organisms in a spatiotemporal-controlled manner. Istradefylline behaves as a bona fide photoinactivatable $A_{2A}R$ antagonist, which could find useful applications to explore the role of localized $A_{2A}R$ in biological, physiological, or behavioral responses in various pathophysiological contexts.

METHODS

Photochemistry—UV−Visible Absorption Spectroscopy. For the determination of the optimal illumination wavelengths, UV−visible absorption spectra were recorded using a Spark microplate reader. Istradefylline samples were prepared at 100 μM in PBS with 0.1% DMSO at room temperature. Samples were measured between 500 and 250 nm with 2 nm fixed intervals in 96-well transparent plates (200 μL of compound solution/well). Illumination at different wavelengths was achieved using a 96-LED plate (LEDA-x, BRC), set at 10 mW.

For the determination of the kinetics and nature of the photoreaction, UV−visible spectra were recorded using a Thermofisher UV−vis spectrophotometer. Samples were prepared with 25 μM istradefylline in PBS with 20% DMSO. Samples were measured between 250 and 600 nm with 2 nm fixed intervals in a quartz cuvette (200 μL of compound solution/cuvette). Illumination at 365 nm was achieved using the CoolLED pE4000 light source, set at 10% intensity (10 mW) or 100% (100 mW).

Estimation of the Cis/Trans/Photoproduct Content by HPLC. For the quantitative analysis of the HPLC chromatogram obtained upon different illumination conditions of the istradefylline samples, the first step was to identify the three isosbestic points (trans−cis, trans-dimers, and cis-dimers). The trans−cis isosbestic point was obtained from the UV−vis spectra of a 25 μM sample of a mixture of only trans and cis isomer, obtained after 5 s of illumination of the sample with 365 nm light (CoolLED pE4000) set at 10 mW. The trans-dimers isosbestic point was obtained from the UV−visible absorption spectrum of trans isomer and pure dimers, obtained, respectively, in the dark and after 10 min of illumination of the same sample with high-power light (100 mW). To obtain the theoretically pure cis absorption spectrum, a 25 μM sample was illuminated for 10 s with 365 nm light set at 10 mW, conditions that mainly lead to the cis isomer. To estimate the proportion of each species in this sample, it was first analyzed by HPLC−MS (see conditions and gradient in the Analytical HPLC−MS & NMR section), and two chromatograms were generated at the wavelengths of the two isosbestic points trans−cis and trans-dimers. For each one, the two peaks corresponding to the two products of the corresponding isosbestic point were integrated to obtain the relative proportion of each. Respecting the trans/cis and the trans/dimers proportion, an estimation of the ratio of dimers and trans and cis isomer was calculated. The pure cis spectrum was then extrapolated, implementing the percentage found for cis and subtracting the effect given by the remaining trans and the percentage of dimers produced in these conditions. From this theoretical cis isomer absorption spectrum, we obtained the cis-dimers isosbestic point used for the calculation of the estimation of cis/trans/dimers content from the different HPLC chromatograms obtained under different illumination conditions.

Analytical HPLC−MS and NMR. Analytical HPLC was performed on a Thermo Ultimate 3000SD (Thermo Scientific Dionex) coupled to a PDA detector and Mass Spectrometer LTQ XL ESI-ion trap (Thermo Scientific) (HPLC-PDA-MS) or on a Waters 2795 Alliance coupled to a Diode array detector (DAD) (Agilent 1100) and an electrospray ionization (ESI) Quattro Micro MS detector (Waters); HPLC columns used were ZORBAX Eclipse Plus C18 (4.6 × 150 mm; 3.5 μm) and ZORBAX Extend-C18 (2.1 × 50 mm, 3.5 μm), respectively.

HPLC purity was determined using the following binary solvent system: A water +0.05% formic acid and B acetonitrile (ACN) with 0.05% formic acid: 5% B for 0.5 min, from 5 to 100% B in 5 min, 100% B for 1.5 min, 100−5% B in 1 min, and 5% B for 2 min (total runtime 10 min). The flow rate was 0.5 mL/min, column temperature was fixed to 35 °C, and wavelengths from 210 to 600 nm were registered.

NMR spectroscopy was performed using a Brüker Avance NEO instrument 400 MHz spectrometer. Chemical shifts are reported in δ (ppm) relative to an internal standard (nondeuterated solvent signal) [chloroform ($CDCl_3$): δ 7.26, 1.56 ppm (^1H), 77.16 ppm (^{13}C)].

Purification of Photoreaction Istradefylline Products. A vial with 10 mg of istradefylline in DMSO (20 mM) was illuminated with 365 nm light (100 mW) for 9 h. The sample was purified by preparative HPLC using a Phenomenex column (00G-4435-N0 Gemini 5u C18 110A 250 × 10.00 mm 5 μm 534461-1), using a flow of 10 mL/min and water/acetonitrile as solvents (+0.05% formic acid) and using a low gradient from 40 to 50% acetonitrile. Three main fractions were obtained named **Dimers 1**, **Dimer 2**, and **Dimer 3**.

Dimers 1, mixture of the anti head-to-tail and head-to-head cyclobutane isomers: 8,8′-((1*r*,2*r*,3*r*,4*r*)-2,4-bis(3,4-dimethoxyphenyl)cyclobutane-1,3-diyl)bis(1,3-diethyl-7-methyl-1*H*-purine-2,6(3*H*,7*H*)-dione) and 8-((1*S*,2*R*,3*R*,4*S*)-2,3-bis(3,4-dimethoxyphenyl)-4-(3-ethyl-1,7-dimethyl-2,6-dioxo-2,3,6,7-tetrahydro-1*H*-purin-8-yl)cyclobutyl)-1,3-diethyl-7-methyl-1*H*-purine-2,6-(3*H*,7*H*)-dione (0,2 mg, 0,130 μmol, 2% yield); ^1H NMR (400 MHz, $CDCl_3$): δ 7.09 (d, *J* = 2.0 Hz, 2H), 6.93−6.88 (m, 2H), 6.84 (d, *J* = 8.3 Hz, 2H), 6.72 (d, *J* = 2.0 Hz, 2H), 6.68 (dd, *J* = 8.3, 2.1 Hz, 2H), 6.55 (d, *J* = 8.2 Hz, 2H), 5.76 (t, *J* = 10.6 Hz, 2H), 4.43 (t, *J* = 9.7 Hz, 2H), 4.24 (app. t, *J* = 9.9 Hz, 4H), 4.21−4.13 (m, 8H), 4.00 (q, *J* = 6.9 Hz, 8H), 3.87 (s, 6H), 3.84 (s, 6H), 3.75 (s, 6H), 3.64 (s, 12H), 3.58 (s, 6H), 1.33 (t, *J* = 7.0 Hz, 12H), 1.21 (t, *J* = 7.0 Hz, 12H).

Dimer 2, syn-head-to-tail cyclobutane isomer: 8-((1*S*,2*S*,3*S*,4*S*)-2,4-bis(3,4-dimethoxyphenyl)-3-(1-ethyl-3,7-dimethyl-2,6-dioxo-2,3,6,7-tetrahydro-1*H*-purin-8-yl)cyclobutyl)-3-ethyl-1,7-dimethyl-1*H*-purine-2,6(3*H*,7*H*)-dione (2,7 mg, 3,51 μmol, 27% yield); ^1H NMR (400 MHz, $CDCl_3$): δ 6.86 (dd, *J* = 8.3, 2.1 Hz, 2H), 6.71 (d, *J* = 8.3 Hz, 2H), 6.66 (d, *J* = 2.1 Hz, 2H), 5.06 (dd, *J* = 9.6, 7.6 Hz, 2H), 4.30 (dd, *J* = 10.0, 7.3 Hz, 2H), 4.21 (q, *J* = 7.0 Hz, 4H), 4.02 (q, *J* = 6.9 Hz, 4H), 3.82 (s, 6H), 3.72 (s, 6H), 3.60 (s, 6H), 1.36 (t, *J* = 7.0 Hz, 6H), 1.21 (t, *J* = 7.0 Hz, 6H).

Dimer 3, syn-head-to-head cyclobutane isomer: 8,8′-((1*R*,2*S*,3*R*,4*S*)-3,4-bis(3,4-dimethoxyphenyl)cyclobutane-1,2-diyl)-bis(1,3-diethyl-7-methyl-1*H*-purine-2,6(3*H*,7*H*)-dione (2,9 mg, 3,77 μmol, 29% yield); ^1H NMR (400 MHz, $CDCl_3$): δ 6.75 (d, *J* = 8.3 Hz, 2H), 6.71 (dd, *J* = 8.3, 1.9 Hz, 2H), 6.41 (d, *J* = 1.9 Hz, 2H), 4.76 (app. d, *J* = 6.4 Hz, 2H), 4.35 (app. d, *J* = 6.4 Hz, 2H), 4.08−3.97 (m, 8H), 3.83 (s, 6H), 3.71 (s, 6H), 3.64 (s, 6H), 1.22 (t, *J* = 7.0 Hz, 6H), 1.17 (t, *J* = 7.0 Hz, 6H).

Cell Culture and Stable Transfection. Chinese hamster ovary FlipIn (FlipIn-CHO) cells obtained from Thermo Fisher Scientific were grown in Ham's F12 medium supplemented with 10% fetal bovine serum (previously inactivated at 55 °C for 30 min). Manipulation and cell culture were done in a biological safety cabinet class 1 and in an incubator at 37 °C, 5% CO_2. Absence of mycoplasma was checked regularly to guarantee the use of mycoplasma-free cells. CHO-$A_{2A}R$ stable cells have been generated using the FlipIn system following the manufacturer's instructions, which allows the generation of an isogenic stable cell line through the guided insertion of the gene at a unique Flp recombinase recognition target (FRT)-site. Briefly, DNA encoding human A_{2A} was inserted in the pcDNA5/FRT-plasmid using cloning sites HindIII and Xho. The ligated DNA was transformed in *Escherichia coli* DH5α competent cells and extracted from different colonies. The integrity of the full plasmid has been checked by sequencing. CHO Flip-In cells have been cotransfected with the pcDNA5/FRT-A_{2A} plasmid and the Flp recombinase vector pOG44 using lipofectamine, according to manufacturer instructions.

https://doi.org/10.1021/acschemneuro.3c00721
ACS Chem. Neurosci. XXXX, XXX, XXX−XXX

The cells having integrated the plasmid into their genome have been selected with hygromycin treatment at 400 μg/mL for 2 weeks. CHO-FlipIn cells stably expressing human $A_{2A}R$ were used in pharmacological experiments.

Cell-Based cAMP Accumulation Assay. CHO cells stably expressing $A_{2A}R$ were seeded in black clear-bottom 96-well plates at a concentration of 10,000 cells/well and incubated at 37 °C and 5% CO_2 for 24 h. cAMP accumulation was estimated using the cAMP Gs HTRF kit (Revvity) according to the manufacturer's instructions. Briefly, 2 μL of istradefylline aliquots were illuminated for different times at 10 mW at 365 nm using a pE4000 CooLED illumination system. Cells were stimulated with the agonist NECA to induce cAMP accumulation while being treated with istradefylline preilluminated under the different light conditions for 20 min at 37 °C. The stimulation buffer also contained adenosine deaminase (0.5 U/mL) to avoid the response induced by ambient adenosine and the PDE IV inhibitor Ro-20-1724 to avoid cAMP degradation. Cells were lysed and transferred to a 384-well plate. The d2-labeled cAMP analogue and the europium cryptate-labeled anti-cAMP antibody were added, and the plate was incubated for 1 h at room temperature. The plate was read using a PheraStar fluorimeter (BMG Labtech) microplate reader. Data were fitted by nonlinear regression and normalized to istradefylline maximal inhibition response (100%) using GraphPad Prism 10 software.

Visualization of Intracellular cAMP Dynamics. To perform these experiments, CHO-$A_{2A}R$ cells were infected by lentivirus encoding the yellow fluorescent cAMP indicator Flamindo2 and a puromycin resistance gene to obtain a polyclonal stable cell line expressing both $A_{2A}R$ and Flamindo2, after selection with 6 μg/mL puromycin. Flamindo2 was a gift from Tetsuya Kitaguchi (Addgene plasmid #73938; http://n2t.net/addgene:73938; RRID: Addgene_73938).[46] 24 h before the experiment, CHO-A_{2A}-Flamindo2 was plated in black clear-bottom 96-well plates at a concentration of 100,000 cells/well and incubated at 37 °C and 5% CO_2. The day after, the medium was changed with the appropriate volume of Functional Drug Screening System (FDSS) buffer containing 1 mM $MgSO_4$, 20 mM N-(2-hydroxyethyl)piperazine-N′-ethanesulfonic acid (HEPES), 3.3 mM Na_2CO_3, 1.3 mM $CaCl_2$, and 0.1% of bovine serum albumin, and cells were incubated for 10 min. The decrease of fluorescence due to cAMP production was assessed using a FDSS/μCELL kinetic plate imager (Hamamatsu) implemented with a custom LED illumination module that allows illuminating 6 × 3 wells at 395 nm directly inside the reading chamber. For the characterization of the CHO-A_{2A}-Flamindo2 stable cell line, 20 μL of 10X NECA solution at increasing concentrations was added after 1 min of baseline, and the subsequent decrease of fluorescence was followed for 6 min. FI signal was monitored at 540 nm after an excitation at 480 nm. A similar protocol was followed to obtain the activity of the three purified fractions of the [2 + 2]-photocycloaddition products obtained. After 1 min of baseline, a 100 μM solution (10×) of the three purified fractions, istradefylline, XAC, or vehicle was injected. FI signal was recorded for 3 min, then 10 μM (10×) of the agonist NECA was injected, and FI was recorded for an additional 8 min. For photopharmacological experiments, the cells were accommodated 10 min at 37 °C with 160 μL/well of FDSS buffer. The experiment started with 1 min of baseline followed by the addition of 20 μL of a 10 μM solution containing either the $A_{2A}R$ antagonists istradefylline or XAC. FI was recorded for 3 min then, recording was stopped during 30 s, during which illumination with 395 nm LED was applied in half of the wells. FI was recorded for 20 s, then 20 μL of a 10 μM solution of the agonist NECA was added, and the fluorescence was recorded for 8 min. For quantitative analysis, the area under the curve after the injection of NECA was determined using GraphPad Prism software.

Behavioral Tests in Zebrafish Larvae (*Danio rerio*). Fish locomotion was measured using a video tracking system (Daniovision, Noldus), equipped with an LED illumination module (385 nm) placed above the observation chamber. We used 5 day postfertilization fish larvae. One zebrafish larva was placed in each well of a 96-well plate (corning Costar) with 75 μL of E3 medium. Thirty min prior to the measurement, the plate was placed inside the observation chamber, previously set at 28 °C, for acclimatization of the fish to the environment. After this period, 75 μL of a 2× solution of the different compounds with 1% DMSO (0.5% DMSO final) was then applied directly into the wells. The preilluminated istradefylline sample was prepared from the 2× solution with an illumination for 2 min at 365 nm at 10 mW (CoolLED, pE4000). The locomotion was recorded 2 min after the addition of the molecules for the duration of the experiment. Zebrafish larvae remained in the dark during the first 30 min and then were submitted to seven cycles of 1 min UV illumination (385 nm, 8 mW) and 1 min in the dark, followed by 10 min in the dark.

Ligands and Chemicals. All chemicals were reagent-grade (Merck, Sigma, Germany, Fluorochem, Ireland). Istradefylline was purchased from MedChemExpress, while NECA and XAC were purchased from Biotechne Tocris. Except when stated otherwise, istradefylline was carefully protected from light during the experiments.

Statistics. All data are reported as mean ± standard error of the mean (±SEM). Number of experiments/animals and statistical tests that were performed on data sets are indicated in figure legends. Data were analyzed with Microsoft excel 2016 and GraphPad Prism softwares v10, using one-way or two-way ANOVA and the appropriate posthoc tests for multiple comparisons. Data were considered significant when $p < 0.05$.

■ ASSOCIATED CONTENT

Supporting Information

The Supporting Information is available free of charge at https://pubs.acs.org/doi/10.1021/acschemneuro.3c00721.

UV−visible absorption spectra; HPLC chromatograms; ^{1}H NMR spectra preorganization of istradefylline for the autophotocycloaddition reaction in solution and the stereochemistry of the products obtained; and summary of relative percentage of cis and trans istradefylline isomers and photocycloaddition products in the illumination conditions corresponding to Figures 2 and 4 (PDF)

■ AUTHOR INFORMATION

Corresponding Authors

Amadeu Llebaria − *MCS, Laboratory of Medicinal Chemistry and Synthesis, Institute of Advanced Chemistry of Catalonia (IQAC-CSIC), 08034 Barcelona, Spain*; Email: amadeu.llebaria@iqac.csic.es

Cyril Goudet − *IGF, Université de Montpellier, CNRS, INSERM, 34094 Montpellier, France*; orcid.org/0000-0002-8255-3535; Email: cyril.goudet@igf.cnrs.fr

Authors

Anaëlle Dumazer − *IGF, Université de Montpellier, CNRS, INSERM, 34094 Montpellier, France; MCS, Laboratory of Medicinal Chemistry and Synthesis, Institute of Advanced Chemistry of Catalonia (IQAC-CSIC), 08034 Barcelona, Spain*

Xavier Gómez-Santacana − *MCS, Laboratory of Medicinal Chemistry and Synthesis, Institute of Advanced Chemistry of Catalonia (IQAC-CSIC), 08034 Barcelona, Spain*; orcid.org/0000-0001-8830-0494

Fanny Malhaire − *IGF, Université de Montpellier, CNRS, INSERM, 34094 Montpellier, France*

Chris Jopling − *IGF, Université de Montpellier, CNRS, INSERM, 34094 Montpellier, France*

Damien Maurel − *IGF, Université de Montpellier, CNRS, INSERM, 34094 Montpellier, France*

https://doi.org/10.1021/acschemneuro.3c00721
ACS Chem. Neurosci. XXXX, XXX, XXX−XXX

Guillaume Lebon − *IGF, Université de Montpellier, CNRS, INSERM, 34094 Montpellier, France*

Complete contact information is available at: https://pubs.acs.org/10.1021/acschemneuro.3c00721

Author Contributions

Conceptualization, AL, GL, and CG; Methodology, XGS, FM, CJ, DM, GL, AL, and CG; Investigation, AD, XGS, FM, and CG; Resources: AL, CJ, DM, GL, and CG; Writing—original draft: AD and CG; Writing—review and editing: all authors; Visualization: AD, XGS, and CG; Funding Acquisition: CG, GL, and AL; Supervision, XGS, CJ, GL, AL, and CG.

Notes

The authors declare no competing financial interest.

■ ACKNOWLEDGMENTS

The authors thank Gavin Fergusson for helpful discussions and critical reading the manuscript, Lourdes Muñoz from SIMChem (IQAC CSIC) for the use of analytical support and helpful discussions, Fabrice Dubois and Stephane Bedut for the development of the custom illumination module for the FDSS/μCELL plate image and the staff of Montpellier Biocampus facilities for their technical help: the PVM facility for the preparation of lentivirus, the Arpege facility for cell-based pharmacological experiments, and the Zefix facility for zebrafish experiments. This work was publicly funded through ANR (the French National Research Agency) under the "Investissements d'avenir" program I-Site MUSE with the reference ANR-16-IDEX-0006 to A.D. and C.G., and the reference ANR-20-CE11-019 to G.L. This work was supported by the Fondation pour la Recherche Médicale, grant number "MND202003011477", to C.G. These results have received funding from European Union's Horizon 2020 research and innovation programme under Marie Skłodowska-Curie grant agreement no. 801342 (Tecniospring INDUSTRY, TECSPR19-1-0062) and the Government of Catalonia's Agency for Business Competitiveness (ACCIÓ) to XGS, Ministerio de Ciencia e Innovación, Agencia Estatal de Investigación and ERDF—A way of making Europe (PCI2018-093047, PID2020-120499RB-I00) to A.L., and the Catalan government (2021 SGR 00508) to A.L. The illustrative graphics were created with http://biorender.com/.

■ REFERENCES

(1) Alexander, S. P. H.; Christopoulos, A.; Davenport, A. P.; et al. The Concise Guide to PHARMACOLOGY 2023/24: G protein-coupled receptors. *Br. J. Pharmacol.* **2023**, *180*, S23−S144.

(2) Hilger, D.; Masureel, M.; Kobilka, B. K. Structure and dynamics of GPCR signaling complexes. *Nat. Struct. Mol. Biol.* **2018**, *25* (1), 4−12.

(3) Hauser, A. S.; Attwood, M. M.; Rask-Andersen, M.; Schiöth, H. B.; Gloriam, D. E. Trends in GPCR drug discovery: new agents, targets and indications. *Nat. Rev. Drug Discovery* **2017**, *16* (12), 829−842.

(4) Santos, R.; Ursu, O.; Gaulton, A.; Bento, A. P.; Donadi, R. S.; Bologa, C. G.; Karlsson, A.; Al-Lazikani, B.; Hersey, A.; Oprea, T. I.; Overington, J. P. A comprehensive map of molecular drug targets. *Nat. Rev. Drug Discovery* **2017**, *16* (1), 19−34.

(5) Ijzerman, A. P.; Jacobson, K. A.; Müller, C. E.; Cronstein, B. N.; Cunha, R. A. International Union of Basic and Clinical Pharmacology. CXII: Adenosine Receptors: A Further Update. *Pharmacol. Rev.* **2022**, *74* (2), 340−372.

(6) Saini, A.; Patel, R.; Gaba, S.; Singh, G.; Gupta, G. D.; Monga, V. Adenosine receptor antagonists: Recent advances and therapeutic perspective. *Eur. J. Med. Chem.* **2022**, *227*, 113907.

(7) Berger, A. A.; Winnick, A.; Welschmeyer, A.; Kaneb, A.; Berardino, K.; Cornett, E. M.; Kaye, A. D.; Viswanath, O.; Urits, I. Istradefylline to Treat Patients with Parkinson's Disease Experiencing "Off" Episodes: A Comprehensive Review. *Neurol. Int.* **2020**, *12* (3), 109−129.

(8) Schwarzschild, M. A.; Agnati, L.; Fuxe, K.; Chen, J.-F.; Morelli, M. Targeting adenosine A2A receptors in Parkinson's disease. *Trends Neurosci.* **2006**, *29* (11), 647−654.

(9) Boknik, P.; Eskandar, J.; Hofmann, B.; Zimmermann, N.; Neumann, J.; Gergs, U. Role of Cardiac A2A Receptors Under Normal and Pathophysiological Conditions. *Front. Pharmacol* **2021**, *11*, 627838.

(10) Sun, C.; Wang, B.; Hao, S. Adenosine-A2A Receptor Pathway in Cancer Immunotherapy. *Front. Immunol.* **2022**, *13*, 837230.

(11) Yu, F.; Zhu, C.; Xie, Q.; Wang, Y. Adenosine A $_{2A}$ Receptor Antagonists for Cancer Immunotherapy: Miniperspective. *J. Med. Chem.* **2020**, *63* (21), 12196−12212.

(12) Sawynok, J. Adenosine receptor targets for pain. *Neuroscience* **2016**, *338*, 1−18.

(13) Merighi, S.; Borea, P. A.; Varani, K.; Vincenzi, F.; Jacobson, K. A.; Gessi, S. A2A Adenosine Receptor Antagonists in Neurodegenerative Diseases. *Curr. Med. Chem.* **2022**, *29* (24), 4138−4151.

(14) Zoghbi, G. J.; Iskandrian, A. E. Adenosine Myocardial Perfusion Imaging. *Curr. Med. Imaging Rev.* **2006**, *2*, 315−327.

(15) Elkholy, K. O.; Hegazy, O.; Okunade, A.; Aktas, S.; Ajibawo, T. Regadenoson Stress Testing: A Comprehensive Review With a Focused Update. *Cureus* **2021**, *13*, No. e12940.

(16) Chen, J.-F.; Cunha, R. A. The belated US FDA approval of the adenosine A2A receptor antagonist istradefylline for treatment of Parkinson's disease. *Purinergic Signalling* **2020**, *16* (2), 167−174.

(17) Dungo, R.; Deeks, E. D. Istradefylline: First Global Approval. *Drugs* **2013**, *73* (8), 875−882.

(18) Shimada, J.; Koike, N.; Nonaka, H.; Shiozaki, S.; Yanagawa, K.; Kanda, T.; Kobayashi, H.; Ichimura, M.; Nakamura, J.; Kase, H.; Suzuki, F. Adenosine A2A antagonists with potent anti-cataleptic activity. *Bioorg. Med. Chem. Lett.* **1997**, *7* (18), 2349−2352.

(19) Orr, A. G.; Lo, I.; Schumacher, H.; Ho, K.; Gill, M.; Guo, W.; Kim, D. H.; Knox, A.; Saito, T.; Saido, T. C.; Simms, J.; Toddes, C.; Wang, X.; Yu, G.-Q.; Mucke, L. Istradefylline reduces memory deficits in aging mice with amyloid pathology. *Neurobiol. Dis.* **2018**, *110*, 29−36.

(20) Lu, J.; Cui, J.; Li, X.; Wang, X.; Zhou, Y.; Yang, W.; Chen, M.; Zhao, J.; Pei, G. An Anti-Parkinson's Disease Drug via Targeting Adenosine A2A Receptor Enhances Amyloid-β Generation and γ-Secretase Activity. *PLoS One* **2016**, *11* (11), No. e0166415.

(21) Hoorens, M. W. H.; Szymanski, W. Reversible, Spatial and Temporal Control over Protein Activity Using Light. *Trends Biochem. Sci.* **2018**, *43* (8), 567−575.

(22) Hüll, K.; Morstein, J.; Trauner, D. In Vivo Photopharmacology. *Chem. Rev.* **2018**, *118* (21), 10710−10747.

(23) Ellis-Davies, G. C. Caged compounds: photorelease technology for control of cellular chemistry and physiology. *Nat. Methods* **2007**, *4* (8), 619−628.

(24) Kobauri, P.; Dekker, F. J.; Szymanski, W.; Feringa, B. L. Rational Design in Photopharmacology with Molecular Photoswitches. *Angew. Chem., Int. Ed.* **2023**, *62* (30), No. e202300681.

(25) Fuchter, M. J. On the Promise of Photopharmacology Using Photoswitches: A Medicinal Chemist's Perspective. *J. Med. Chem.* **2020**, *63* (20), 11436−11447.

(26) Welleman, I. M.; Hoorens, M. W. H.; Feringa, B. L.; Boersma, H. H.; Szymański, W. Photoresponsive molecular tools for emerging applications of light in medicine. *Chem. Sci.* **2020**, *11* (43), 11672−11691.

(27) Ricart-Ortega, M.; Font, J.; Llebaria, A. GPCR photopharmacology. *Mol. Cell. Endocrinol.* **2019**, *488*, 36−51.

(28) Wijtmans, M.; Josimovic, I.; Vischer, H. F.; Leurs, R. Optical control of Class A G protein-coupled receptors with photoswitchable ligands. *Curr. Opin. Pharmacol.* **2022**, *63*, 102192.
(29) Donthamsetti, P. C.; Winter, N.; Schönberger, M.; Levitz, J.; Stanley, C.; Javitch, J. A.; Isacoff, E. Y.; Trauner, D. Optical Control of Dopamine Receptors Using a Photoswitchable Tethered Inverse Agonist. *J. Am. Chem. Soc.* **2017**, *139* (51), 18522−18535.
(30) Westphal, M. V.; Schafroth, M. A.; Sarott, R. C.; Imhof, M. A.; Bold, C. P.; Leippe, P.; Dhopeshwarkar, A.; Grandner, J. M.; Katritch, V.; Mackie, K.; Trauner, D.; Carreira, E. M.; Frank, J. A. Synthesis of Photoswitchable Δ^{9} -Tetrahydrocannabinol Derivatives Enables Optical Control of Cannabinoid Receptor 1 Signaling. *J. Am. Chem. Soc.* **2017**, *139* (50), 18206−18212.
(31) Rodriguez-Soacha, D. A.; Steinmuller, S. A. M.; Isbilir, A.; Fender, J.; Deventer, M. H.; Ramirez, Y. A.; Tutov, A.; Sotriffer, C.; Stove, C. P.; Lorenz, K.; Lohse, M. J.; Hislop, J. N.; Decker, M. Development of an Indole-Amide-Based Photoswitchable Cannabinoid Receptor Subtype 1 (CB(1)R) "Cis-On" Agonist. *ACS Chem. Neurosci.* **2022**, *13* (16), 2410−2435.
(32) Banghart, M. R.; Sabatini, B. L. Photoactivatable Neuropeptides for Spatiotemporally Precise Delivery of Opioids in Neural Tissue. *Neuron* **2012**, *73* (2), 249−259.
(33) Schönberger, M.; Trauner, D. A Photochromic Agonist for μ-Opioid Receptors. *Angew. Chem., Int. Ed.* **2014**, *53* (12), 3264−3267.
(34) Gomez-Santacana, X.; Panarello, S.; Rovira, X.; Llebaria, A. Photoswitchable allosteric modulators for metabotropic glutamate receptors. *Curr. Opin. Pharmacol.* **2022**, *66*, 102266.
(35) Duran-Corbera, A.; Faria, M.; Ma, Y.; Prats, E.; Dias, A.; Catena, J.; Martinez, K. L.; Raldua, D.; Llebaria, A.; Rovira, X. A Photoswitchable Ligand Targeting the β_1 -Adrenoceptor Enables Light-Control of the Cardiac Rhythm. *Angew. Chem., Int. Ed.* **2022**, *61* (30), No. e202203449.
(36) Bosma, R.; Dijon, N. C.; Zheng, Y.; Schihada, H.; Hauwert, N. J.; Shi, S.; Arimont, M.; Riemens, R.; Custers, H.; van de Stolpe, A.; Vischer, H. F.; Wijtmans, M.; Holliday, N. D.; Kuster, D. W. D.; Leurs, R. Optical control of the β2-adrenergic receptor with optoprop-2: A cis-active azobenzene analog of propranolol. *iScience* **2022**, *25* (9), 104882.
(37) Taura, J.; Nolen, E. G.; Cabré, G.; Hernando, J.; Squarcialupi, L.; López-Cano, M.; Jacobson, K. A.; Fernández-Dueñas, V.; Ciruela, F. Remote control of movement disorders using a photoactive adenosine A2A receptor antagonist. *J. Controlled Release* **2018**, *283*, 135−142.
(38) Bahamonde, M. I.; Taura, J.; Paoletta, S.; Gakh, A. A.; Chakraborty, S.; Hernando, J.; Fernández-Dueñas, V.; Jacobson, K. A.; Gorostiza, P.; Ciruela, F. Photomodulation of G Protein-Coupled Adenosine Receptors by a Novel Light-Switchable Ligand. *Bioconjugate Chem.* **2014**, *25* (10), 1847−1854.
(39) Hüll, K.; Fernández-Dueñas, V.; Schönberger, M.; López-Cano, M.; Trauner, D.; Ciruela, F. Optical Control of Adenosine-Mediated Pain Modulation. *Bioconjugate Chem.* **2021**, *32* (9), 1979−1983.
(40) Hockemeyer, J.; Burbiel, J. C.; Müller, C. E. Multigram-Scale Syntheses, Stability, and Photoreactions of A_{2A} Adenosine Receptor Antagonists with 8-Styrylxanthine Structure: Potential Drugs for Parkinson's Disease. *J. Org. Chem.* **2004**, *69* (10), 3308−3318.
(41) Nonaka, Y.; Shimada, J.; Nonaka, H.; Koike, N.; Aoki, N.; Kobayashi, H.; Kase, H.; Yamaguchi, K.; Suzuki, F. Photoisomerization of a potent and selective adenosine A2 antagonist, (E)-1,3-dipropyl-8-(3,4-dimethoxystyryl)-7-methylxanthine. *J. Med. Chem.* **1993**, *36* (23), 3731−3733.
(42) Petzer, J. P.; Steyn, S.; Castagnoli, K. P.; Chen, J.-F.; Schwarzschild, M. A.; Van der Schyf, C. J.; Castagnoli, N. Inhibition of monoamine oxidase B by selective adenosine A 2A receptor antagonists. *Bioorg. Med. Chem.* **2003**, *11* (7), 1299−1310.
(43) Meier, H. The Photochemistry of Stilbenoid Compounds and Their Role in Materials Technology. *Angew. Chem., Int. Ed.* **1992**, *31* (11), 1399−1420.
(44) Vedernikov, A. I.; Kuz'mina, L. G.; Sazonov, S. K.; Lobova, N. A.; Loginov, P. S.; Churakov, A. V.; Strelenko, Y. A.; Howard, J. A. K.; Alfimov, M. V.; Gromov, S. P. Styryl dyes. Synthesis and study of the solid-state [2 + 2] autophotocycloaddition by NMR spectroscopy and X-ray diffraction. *Russ. Chem. Bull.* **2007**, *56* (9), 1860−1883.
(45) Ben-Efraim, D. A.; Green, B. S. The use of mid-points or average NMR chemical shifts in stereochemical assignments. *Tetrahedron* **1974**, *30*, 2357−2364.
(46) Odaka, H.; Arai, S.; Inoue, T.; Kitaguchi, T. Genetically-Encoded Yellow Fluorescent cAMP Indicator with an Expanded Dynamic Range for Dual-Color Imaging. *PLoS One* **2014**, *9* (6), No. e100252.
(47) Gómez-Santacana, X.; Pittolo, S.; Rovira, X.; Lopez, M.; Zussy, C.; Dalton, J. A. R.; Faucherre, A.; Jopling, C.; Pin, J.-P.; Ciruela, F.; Goudet, C.; Giraldo, J.; Gorostiza, P.; Llebaria, A. Illuminating Phenylazopyridines To Photoswitch Metabotropic Glutamate Receptors: From the Flask to the Animals. *ACS Cent. Sci.* **2017**, *3* (1), 81−91.
(48) Boehmler, W.; Petko, J.; Woll, M.; Frey, C.; Thisse, B.; Thisse, C.; Canfield, V. A.; Levenson, R. Identification of zebrafish A2 adenosine receptors and expression in developing embryos. *Gene Expression Patterns* **2009**, *9* (3), 144−151.
(49) Ohno, Y.; Suzuki, M.; Asada, H.; Kanda, T.; Saki, M.; Miyagi, H.; Yasunaga, M.; Suno, C.; Iwata, S.; Saito, J.-i.; Uchida, S. In Vitro Pharmacological Profile of KW-6356, a Novel Adenosine A_{2A} Receptor Antagonist/Inverse Agonist. *Mol. Pharmacol.* **2023**, *103* (6), 311−324.
(50) Santos, L. C.; Ruiz-Oliveira, J.; Silva, P. F.; Luchiari, A. C. Caffeine Dose-Response Relationship and Behavioral Screening in Zebrafish. In *The Question of Caffeine*; Latosinska, J. N., Latosinska, M., Eds.; InTech, 2017.
(51) Rovira, X.; Trapero, A.; Pittolo, S.; Zussy, C.; Faucherre, A.; Jopling, C.; Giraldo, J.; Pin, J.-P.; Gorostiza, P.; Goudet, C.; Llebaria, A. OptoGluNAM4.1, a Photoswitchable Allosteric Antagonist for Real-Time Control of mGlu 4 Receptor Activity. *Cell Chem. Biol.* **2016**, *23* (8), 929−934.
(52) Ito, Y.; Kajita, T.; Kunimoto, K.; Matsuura, T. Accelerated photodimerization of stilbenes in methanol and water. *J. Org. Chem.* **1989**, *54* (3), 587−591.
(53) Kirchner, S.; Leistner, A. L.; Godtel, P.; Seliwjorstow, A.; Weber, S.; Karcher, J.; Nieger, M.; Pianowski, Z. Hemipiperazines as peptide-derived molecular photoswitches with low-nanomolar cytotoxicity. *Nat. Commun.* **2022**, *13* (1), 6066.
(54) Willems, S.; Morstein, J.; Hinnah, K.; Trauner, D.; Merk, D. A Photohormone for Light-Dependent Control of PPARα in Live Cells. *J. Med. Chem.* **2021**, *64* (14), 10393−10402.
(55) Gao, L.; Meiring, J. C. M.; Varady, A.; Ruider, I. E.; Heise, C.; Wranik, M.; Velasco, C. D.; Taylor, J. A.; Terni, B.; Weinert, T.; Standfuss, J.; Cabernard, C. C.; Llobet, A.; Steinmetz, M. O.; Bausch, A. R.; Distel, M.; Thorn-Seshold, J.; Akhmanova, A.; Thorn-Seshold, O. In Vivo Photocontrol of Microtubule Dynamics and Integrity, Migration and Mitosis, by the Potent GFP-Imaging-Compatible Photoswitchable Reagents SBTubA4P and SBTub2M. *J. Am. Chem. Soc.* **2022**, *144* (12), 5614−5628.
(56) Schmidt, D.; Rodat, T.; Heintze, L.; Weber, J.; Horbert, R.; Girreser, U.; Raeker, T.; Bußmann, L.; Kriegs, M.; Hartke, B.; Peifer, C. Axitinib: A Photoswitchable Approved Tyrosine Kinase Inhibitor. *ChemMedChem* **2018**, *13* (22), 2415−2426.
(57) Onoue, S.; Tsuda, Y. Analytical studies on the prediction of photosensitive/phototoxic potential of pharmaceutical substances. *Pharm. Res.* **2006**, *23* (1), 156−164.
(58) Kim, W. B.; Shelley, A. J.; Novice, K.; Joo, J.; Lim, H. W.; Glassman, S. J. Drug-induced phototoxicity: A systematic review. *J. Am. Acad. Dermatol.* **2018**, *79* (6), 1069−1075.
(59) El Ouardi, M.; Tamarit, L.; Vaya, I.; Miranda, M. A.; Andreu, I. Cellular photo(geno)toxicity of gefitinib after biotransformation. *Front. Pharmacol* **2023**, *14*, 1208075.
(60) Bhurta, D.; Bharate, S. B. Styryl Group, a Friend or Foe in Medicinal Chemistry. *ChemMedChem* **2022**, *17* (7), No. e202100706.

https://doi.org/10.1021/acschemneuro.3c00721
ACS Chem. Neurosci. XXXX, XXX, XXX−XXX